# Diffusion of Polystyrene in Controlled Pore Glasses: Transition from the Dilute to the Semidilute Regime

**Iwao Teraoka,* Kenneth H. Langley,† and Frank E. Karasz**

*Department of Polymer Science and Engineering, University of Massachusetts, Amherst, Massachusetts 01003*

*Received May 20, 1992; Revised Manuscript Received October 16, 1992*

ABSTRACT: The diffusion of polystyrene molecules inside controlled pore glasses with inert pore walls was investigated by the technique of dynamic light scattering over a wide range of concentrations of dissolved polystyrene in solutions in equilibrium with the porous glasses immersed in them. Index-matching of the solvent to the silica glasses effectively facilitates the acquisition of information on the dynamics of polymer chains inside the pore network without being compromised by multiple scattering of photons. When the solute concentration outside the pore is much smaller than the overlap concentration $\nu^*$, the apparent diffusion coefficient $D_{pore}$ of polymers within the pore shows little dependence on concentration, a result indicating the realization of a well-defined dilute regime inside the pore. As the outside concentration increases and approaches $\nu^*$, $D_{pore}$ rapidly increases. This tendency is more pronounced for polystyrene samples that have higher molecular weights and are predicted to have a lower partition coefficient and hence a lower concentration inside the pore. With further increases of concentration beyond $\nu^*$, $D_{pore}$ approaches the apparent diffusion coefficient outside the pore. Moreover, $D_{pore}$ becomes almost the same for the three different molecular weights of polystyrene fractions studied and depends primarily on the weight concentration of the solute outside the pore. These features are typical of a semidilute solution regime for flexible polymers characterized by a correlation length $\xi$ for monomer concentration fluctuations. The value of $\xi$ calculated from $D_{pore}$ is much smaller than the pore radius. The rapid increase in the diffusion coefficient is ascribed to a drastic increase of the polymer concentration inside the pore, which results from an equilibration of the chemical potential of the polymer molecule between the interior of the pore and the exterior. Thus, when the concentration exceeds $\nu^*$, the osmotic pressure outside the pore increases rapidly and hence the chain tends to be squeezed into a pore even at the expense of reduced entropy. We present a quantitative analysis of this highly nonlinear partitioning of polymer molecules.

## Introduction

The statics and dynamics of polymer chains in a confining geometry such as a porous medium have attracted increased interest in recent years because of the wide range of applications of porous media, e.g., to catalysts, chromatography, and membrane filtration. Interest has been focused on the interplay between a characteristic length of the polymeric system and that of the porous medium. The porous medium provides the polymers with geometrical hindrance including excluded-volume effects and hydrodynamic interactions as well as various kinds of surface-specific interactions. It is important, as a basis of the applications, to understand which of these interactions is responsible for specific equilibrium and transport properties that we obtain or expect to obtain from the porous medium. It should also be noted that an increasing variety of porous media with different materials, processing, and pore architectures is becoming available and is being applied to secondary products, often without a thorough comprehension of the properties and structures of the media.

The study of polymer solutions in porous media, on which we report in this contribution, is not new. Size-exclusion chromatography[1,2] (SEC) has been widely used to characterize a molecular weight distribution of polymers and to prepare polymer fractions from a polydisperse sample.[2,3] As porous media, either chemically cross-linked gels fully swollen with solvent or silica glass fragments composed of a highly interconnected network of pore and a solid silica phase have been used to provide geometrical restrictions of the polymer molecule. In either porous medium, the principle of SEC is based on a difference of the partition coefficient between the interior of the pore and the exterior by varying the size of the polymer chains in solution. SEC works well once it is calibrated. However, we do not have, even now, enough information on the mechanisms of SEC as the basis for further improvement of the technique.

The studies[4-19] of the dynamics of polymer molecules inside the pore have been focused so far on the extent of reduction in the diffusion coefficient of the polymer molecule compared with that in free solutions and on the dependence of this reduction on polymer chain length and pore size. Transport properties of polymer molecules through track-etched membranes that have straight cylindrical pores across their thickness were investigated.[4-9,11] Without exception the transport was found to become slower as the size of the polymer chain becomes larger. It was also found that star-branched polymers exhibited flow characteristics well explained by existing theories[20] for hard spheres but the transport of linear-chain polymers were less restricted than star-branched polymers of the same coil radius in free solutions.[7] The effect of convection on the transport coefficient was also studied.[10,19]

Recently our group[12-17] employed the technique of dynamic light scattering (DLS) to observe the motion of polymer molecules in a small volume inside the pore filled with polymer solution. This technique utilizes the advantage of index-matching of the solvent to the porous glass, thus enabling us to detect the motion of polymers without interference from the multiple scattering of photons.[13] DLS has an advantage in that it observes directly a small portion of polymer solutions inside the pore that is quiescent and in equilibrium with the solutions outside the pore. It was found that the polymer molecules follow diffusion dynamics in highly connected networks of pores and that the diffusion coefficient drastically reduces as the coil radius exceeds the pore radius.

† Department of Physics and Astronomy, University of Massachusetts, Amherst, MA 01003.

0024-9297/93/2226-0287$04.00/0 

The concentration dependence of the diffusion coefficient inside the pore has also been studied[13,14] using DLS for solutions much more dilute than the overlap concentration. The concentration dependence of the diffusion coefficient was found to be greater in the interior of the pore than in the exterior. This greater concentration dependence was ascribed to an enhanced interaction between chains in a narrow channel of low dimensionality.[13,14]

A similar phenomenon was reportedly observed in membrane transport of polymer molecules in solutions.[4,5,8,9] A transition behavior in the transport coefficient was found with increases of the polymer concentration. Transport in the semidilute solution became as much as 2 orders of magnitude faster than for the dilute solution case. This enhancement was ascribed to the increase in the osmotic pressure.

In this contribution, we report on the dynamics of linear-chain polymers inside a porous glass bead over a wide range of concentrations of polymer solutions in contact with the porous glass. There are at least two relevant aspects of the concentration effect on the dynamics of polymer chains in the pore.

The first is an effect of low dimensionality on the dynamics as proposed by Bishop et al.[13] In free solutions in three dimensions, macromolecules in a good solvent exert a repulsive force on each other, which results in an increased mutual diffusion coefficient as the concentration increases. Inside pores this effect is expected to be more prominent when the polymer size becomes comparable to or larger than the pore size.

The second aspect is a possible nonlinear partitioning of polymer chains between the interior of the pore and the exterior. A deviation from the proportionality between the polymer concentration in the interior and that in the exterior is here referred to as a nonlinear partitioning. The first studies of this nonlinear effect[21,22] were based on the idea that chain contraction in the semidilute regime might increase the partition coefficient. Then the effect was studied in computer simulations[23-25] and in experiments[26] for polymer chains in the range below the overlap concentration. The studies found that the partition coefficient increases as the polymer concentration increases and that the increase is larger for a longer polymer chain. The concentration effect should be drastic in a more concentrated range. As predicted by Brochard et al.[27,28] for polymer chains with extension much larger than the pore size, the partitioning between the interior of the pore and the exterior should exhibit a transition from a weak to a strong penetration regime as the concentration outside the pore exceeds a threshold value. If this transition also applies to polymer chains not so large relative to pore size (this condition is necessary so that there is a reasonable number of polymer molecules inside the pore when the concentration outside is dilute), then we should be able to observe the transition by DLS. It is well-known[29-33] that in bulk solution the autocorrelation function of the concentration fluctuations observed in DLS shows a crossover from that corresponding to a mutual diffusion to that related to the cooperative dynamics of local concentration fluctuations as the solute concentration exceeds the overlap concentration. It is of interest to observe the counterpart in polymer solutions within the pore. For example, such a transition might lead to an explanation of the "overload" effect in SEC in which the retention time displays a tail at longer times when the concentration of the injected sample is too high.

The organization of this contribution is as follows. First, we present the theoretical background on the diffusion coefficient observed in DLS for free polymer solutions and on the static properties of polymers in the pore. Then we explain details of sample preparation, the DLS experiment, and data analysis. We show experimental results for polystyrene samples of three different molecular weights. The results, which cover a wide range of concentrations including the overlap concentration, will be shown separately for free solutions and for solutions in porous glasses. Having discussed the apparent diffusion coefficient of polymer solutions in the interior and the exterior of the pore, we propose a quantitative theory for the partition coefficient over a wide range of concentrations and compare it with the experimental results.

## Theoretical Background

**Diffusion Coefficient in Free Solutions.** Polymers in good solvents exhibit different dynamic properties in dilute, $\nu \ll \nu^*$, and semidilute, $\nu \gg \nu^*$, regimes, where $\nu$ is the polymer concentration, i.e., number of polymer molecules per unit volume, and $\nu^*$ is the overlap concentration defined by[34]

$$\nu^*(\sqrt{2}R_g)^3 = 1 \tag{1}$$

where $R_g$ is the radius of gyration of the polymer molecule. Slightly different numerical coefficients have been used to define $\nu^*$. The definition here gives a radius about 48% larger than the value defined by the other commonly used equation $(4\pi/3)R_g^3\nu^* = 1$.[33,35] We employ the definition of eq 1 for consistency in the later parts of this contribution.

The dynamic light scattering experiment directly observes concentration fluctuations in $\mathbf{k}$-space, where $\mathbf{k}$ is the relevant wavevector. From the experimental results of DLS on a polymeric system, we can determine whether the system follows a diffusion equation or not. The criterion is whether the initial decay constant $\Gamma(\mathbf{k})$ in the autocorrelation function (defined later) is proportional to $\mathbf{k}^2$ in the long wavelength limit to produce the apparent diffusion coefficient $D_{app}$, i.e., whether $D_{app} = \lim_{\mathbf{k}\to 0}(\Gamma(\mathbf{k})/\mathbf{k}^2)$ exists or not. See a textbook[35] for derivation of this relation.

The picture of concentration fluctuation is different between dilute and semidilute regimes, and therefore the meaning of $D_{app}$ depends on the concentration range. When $\nu \ll \nu^*$, on the one hand, the fluctuation refers to the center of mass position of the chain in the long wavelength limit: $|\mathbf{k}|R_g \ll 1$. The apparent diffusion coefficient $D_{app}$ is then identified as the mutual diffusion coefficient $D_m$ of the center of mass. They are related by $D_{app} = (1 - \phi)D_m$,[36] where $\phi$ is the volume fraction occupied by the polymer molecules in the solution. The correction due to solvent backflow[37,38] is negligible; i.e., $1 - \phi \cong 1$ when $\nu \ll \nu^*$.

In the dilute solution limit, the mutual diffusion coefficient reduces to the self-diffusion coefficient $D_0$ of an isolated polymer molecule, i.e.

$$D_0 = \frac{k_B T}{6\pi\eta R_H} \tag{2}$$

where $k_B$ is the Boltzmann constant, $T$ is the absolute temperature, $\eta$ is the solvent viscosity, and $R_H$ is the hydrodynamic radius of the polymer molecule. To relate $R_H$ to the radius of gyration $R_g$, it is convenient to employ an expression obtained by Oono and Kohmoto[39] for an isolated chain in a good solvent on the basis of renormalization group theory: $D_0 = 0.2030k_BT/(\sqrt{6}\eta R_g)$. Together with eq 2, we find that $R_g/R_H = 1.562$. Another

characteristic length is the root mean square of the end-to-end distance $R_F$, which is related to $R_g$ by $R_F/R_g = 2.510$.[40,41]

A deviation of $D_m$ from $D_0$ when $\nu/\nu^* \ll 1$ is usually expressed in linear form:

$$D_m \simeq D_0(1 + k_D\nu/\nu^*) \quad (3)$$

The coefficient $k_D$ is usually positive for polymer molecules in good solvent.

When $\nu \gg \nu^*$, on the other hand, the chains are overlapped, and the correlation length $\xi$ of the concentration fluctuation is smaller than the coil radius. Note that $\xi$ is a function of the monomer concentration $\rho$ alone ($\rho = N\nu$, with $N$ being the number of monomers in a chain). The apparent diffusion coefficient is then related to a cooperative diffusion coefficient $D_C$:

$$D_{app} = (1 - \phi)D_C = (1 - \phi)\frac{k_BT}{6\pi\eta\xi} \quad (4)$$

Scaling arguments yield

$$\xi \sim \rho^{-x} \quad (5)$$

with the exponent $x = 0.75$ for polymers in a good solvent in the semidilute regime ($\rho \ll 1$). In the $\Theta$ solvent this exponent is 0.5. If the chains are not sufficiently long or if the solvent is not "good" enough, then the exponents obtained in the DLS experiments are smaller than 0.75.[33]

**Polymer Chains in a Pore.** When a porous medium is in contact with a solution containing polymer molecules, the vacant space of the medium (i.e., the pore space) is filled with the polymer solution. The concentration $\nu_{in}$ of the polymer inside the pore is always smaller than the concentration $\nu_{out}$ in the bulk solution. The inner walls of the porous medium can often be assumed to be inert, which means that there is no adsorption of polymer chains onto the wall. When $\nu_{out} \ll \nu^*$ and the interaction between different chains is negligible, $\nu_{in}$ is proportional to $\nu_{out}$ (linear partitioning). In the dilute limit, the partition coefficient $p_I$ defined by $p_I \equiv \nu_{in}/\nu_{out}$ reduces to a value $p_0$ determined purely by a decrease of entropy $\Delta S$ of the polymer chain confined in the pore with respect to the chain in the bulk solution:

$$p_I \simeq p_0 = \exp(-\Delta S/k_B) \quad (6)$$

From the definition, $\Delta S$ is determined by the number of conformations available to the polymer chains in the interior of the pore compared with that in the exterior.

An exact formulation for $p_0$ was carried out for a Gaussian coil[42] and some geometrically simple rigid bodies[43] in a straight cylindrical pore that mimics the pore in controlled pore glasses at least over a short distance. Casassa[42] obtained $p_0$ for a Gaussian coil with a radius of gyration $R_g$ confined in a cylinder with radius $R_P$:

$$p_0 = f_P(R_g/R_P) \quad (7)$$

where

$$f_P(x) = 4\sum_{m=1}^{\infty}\frac{1}{\beta_m^2}\exp(-\beta_m^2x^2) \quad (8)$$

where $\beta_m$ ($m = 1, 2, ...$) is the $m$th root of the zeroth-order Bessel function $J_0(\beta) = 0$. A numerical calculation gives $f_P(1) \simeq 0.0022$, for example.

For a real chain in a good solvent, however, a scaling theory[27,28,44,45] has been presented so far only for a chain with an extension much larger than the pore size. The scope of our present work is for polymer chains that have extensions not too large compared with the pore size and hence do not qualify as chains to which the scaling theory is expected to apply. The theoretical argument we develop later in this contribution, however, does have some results in common with the scaling theory. Therefore, we briefly review the results of the scaling theory.

1. A polymer chain is considered to consist of $N$ monomers of size $a$. For a chain with the end-to-end distance $R_F = aN^{3/5} \gg d_P$, where $d_P = 2R_P$ is the pore diameter, the partition coefficient is given as $\ln p_0 \simeq -N(a/d_P)^{5/3}$.

2. The chain is elongated in the pore like an array of blobs of diameter $d_P$. The extension along the pore $R_\parallel$ is given as

$$R_\parallel \simeq aN(a/d_P)^{2/3} \quad (9)$$

3. Overlapping of chains in the pore occurs when the cylinder is filled with rods of length $R_\parallel$. Overlap monomer concentration $\rho_{in}^*$ (number of monomers per unit volume of pore space) inside the pore does not depend on $N$: $\rho_{in}^* \simeq N/(d_P^2R_\parallel) \simeq a^{-3}(a/d_P)^{4/3}$.

4. The correlation length $\xi$ is independent of $N$ in the pore when $\rho_{in} > \rho_{in}^*$ and given as $\xi \simeq d_P(\rho_{in}^*/\rho_{in})^{3/4}$.

5. The osmotic pressure $\Pi$ in the pore has the same dependence on the filling ratio $\phi_{in} = \rho_{in}a^3$ as that in the bulk solution: $\Pi = (k_BT/a^3)\phi_{in}^{9/4}$.

6. The partition coefficient shows a transition from a weak to a strong penetration regime as the polymer concentration $\nu_{out}$ of the bulk solution in equilibrium with the pore exceeds $\nu_{in}^*$. This threshold concentration is given by the condition that the correlation length outside the pore be comparable to the pore diameter. Note that in terms of monomer concentration $\rho_{in}^* \geq \rho_{out}^*$ always holds for a varying chain length, because $\rho_{in}^* = \rho_{out}^*$ for a chain with $R_F \leq d_P$, and $\rho_{out}^*$ scales as $R_F^{-4/3}$ while $\rho_{in}^*$ does not depend on $R_F$ for a chain with $R_F \geq d_P$.

## Experimental Section

**Dynamic Light Scattering Measurements.** Dynamic light scattering measurements were performed by using a 5-mW He–Ne laser (Melles-Griot) as the light source. The laser beam was focused on the center of a test tube that held the sample solution and the porous glass bead. The cell holder was constructed to allow the measurement of light intensity scattered at several different fixed angles between 15° and 155° with axes tilted by 5° from the horizontal to diminish stray light. The autocorrelation function (ACF) of the photon-counting pulse was measured using a Langley–Ford Instruments Model 1096 digital correlator (Coulter Electronics) equipped with a 4-bit correlator of 256 main channels equally spaced by the sampling time $\Delta t$. An additional 16 channels can be delayed by $1024\Delta t$ with reference to the main channels for measurement of the base line.

The photon-counting signal from the free solutions of polymers at a scattering vector $\mathbf{k}$ gives the intensity ACF $C(\mathbf{k},t)$ for the delay time $t$ in the homodyne (or self-beating) configuration as $C(\mathbf{k},t) = B[1 + f_{HO}g_1^2(\mathbf{k},t)]$, where $B$ is the base-line value, $f_{HO}$ is a coherence factor smaller than unity, and $g_1(\mathbf{k},t)$ is related to the normalized electric field correlation function $g_E(\mathbf{k},t)$ by a Siegert relation $g_1(\mathbf{k},t) = |g_E(\mathbf{k},t)|$.[46] The magnitude of $\mathbf{k}$ is expressed as $k \equiv |\mathbf{k}| = (4\pi n/\lambda)\sin(\theta/2)$, where $n$ is the refractive index of the solvent (1.471 at 40.7 °C), $\lambda$ the wavelength of incident beam in vacuum (632.8 nm), and $\theta$ the scattering angle.

In the DLS measurement of the chain dynamics inside the pore, a technique of index-matching between the silica glass and the solvent was used to eliminate multiple scattering events.[13] The photon stream coming from the porous glass bead immersed in the polymer solution comprises two components. One is a photon flux scattered by the immobile silica glass. The other is a photon flux scattered by the polymer molecule moving in the immobile network of the porous glass. Even in the optimal condition of index-matching between the silica and the solvent, the scattered light comes mostly from the silica in the porous

**Table I**
**Characterization of Polystyrene Samples**

| sample | $M_p$ | $D_0 \times 10^{11}$/m$^2$ s$^{-1}$ | $R_H$/nm[a] | $R_g$/nm[a] | $c^*$/mg mL$^{-1}$ [a] |
|---|---|---|---|---|---|
| PS035 | 35 000 | 9.93 | 4.34 | 6.78 | 53.8 |
| PS170 | 170 000 | 4.01 | 10.7 | 16.8 | 21.1 |
| PS949 | 949 000 | 1.48 | 29.1 | 45.4 | 5.95 |

[a] Calculated.

glass, because of the inhomogeneity of the glass bead. These photons serve as a local oscillator in this optical mixing configuration (homodyne–heterodyne[47] or simply heterodyne). Then, the ACF of the signal detected by the photomultiplier tube consists of a component of squared light intensity $I_{LO}^2$ scattered by the glass alone, which is static, and a component proportional to the scattering intensity from the polymer molecules $\langle I_S \rangle$ and that from the silica $I_{LO}$.[13] The first component is much larger than the second one. There is also a third component proportional to $\langle I_S \rangle^2 g_1^2(\mathbf{k},t)$ coming from the polymer molecules, but this component is usually negligible relative to the second term. Then, the detected ACF $C(\mathbf{k},t)$ is expressed as $C(\mathbf{k},t) = B[1 + f_{HE} g_1(\mathbf{k},t)]$,[47] with a heterodyne coherence factor

$$f_{HE} = \frac{2\langle I_S \rangle}{I_{LO}} f_C \tag{10}$$

where a coherence factor $f_C$ depends on the degree of wavefront matching between the local oscillator and the light scattered by the polymer molecule at the photomultiplier tube receptor surface.[47] In our experiments the coherence factor always satisfied strong heterodyne limit $f_{HE} \ll 1$.

**Samples.** Polystyrene standards of three different molecular weights PS035, PS170, and PS949 (Pressure Chemical) were used. The manufacturer-supplied information on the peak molecular weight $M_p$ is listed in Table I. The polydispersity index $M_w/M_n$, where $M_w$ and $M_n$ are the weight-average and number-average molecular weights, is less than 1.06. We used 2-fluorotoluene (2FT) as solvent (Aldrich) without further treatment. 2-Fluorotoluene is a good solvent for polystyrene[13] and also provides adequate index-matching with silica. The partial volume[34] of polystyrene in 2FT was assumed to be 0.152 nm$^3$/monomer unit, a value obtained for polystyrene in benzene at room temperature.[48]

The porous silica glass beads used in this study are the same as those used in our laboratory previously and were designated as G275. They comprise bicontinuous phases of solid silica and pore volume. Over a short distance, the pore configuration resembles a cylinder. Because the beads were made in a spinodal decomposition process, the pore size distribution is uniform, and there is a well-defined pore radius. The glass beads were supplied by Shell Development Co. The nominal pore radius $R_P$ is 275 Å, and the pore volume is 1.3 cm$^3$/g; the bead diameter is between 1.0 and 1.5 mm. To avoid any specific surface interaction between the pore walls and the polymer molecules, the surface hydroxyl moieties inside the glass beads were replaced by (trimethylsilyl)-oxy units (silanization).[13] The beads were dried in vacuum at ca. 100 °C prior to use.

In the experiments, a silanized glass bead was mounted on top of a FEP (du Pont) tube located at the center of a dust-free test tube of inner diameter ca. 8 mm. A polymer solution was then introduced into the test tube through a Teflon membrane filter (0.22-μm pore size; Millipore Millex FGS). The test tube was sealed to prevent solvent evaporation. At least a week was allowed to pass before DLS measurements. The pore volume is about 3 orders of magnitude smaller than the volume of the polymer solution in the test tube. Therefore, the porous glass bead does not alter the polymer concentration in the solution outside the pore. To achieve good index-matching between the test tube, the solvent, and the glass bead, all the measurements were performed with the test tube immersed in decalin at 40.7 ± 0.1 °C.

The concentration of polystyrene in the porous glass for a given concentration outside the pore cannot be easily estimated. A small partition coefficient makes it difficult to measure the interior concentration. The partition coefficients are known only for perfectly rigid bodies of simple geometrical shape and for Gaussian chains confined in cavities of simple geometry, e.g., cylinder, parallel-plane slit, and sphere. The porous glasses used have a much more complicated and random network structure. Moreover, the partition coefficient depends on the concentration of polymers outside the pore, as will be discussed later in this contribution.

**Data Analysis.** Diffusion coefficients of the polystyrene fraction in free solution were measured at three scattering angles: 15.8°, 25.5°, and 35.3°. The sampling time $\Delta t$ was selected so that $\ln g_1^2(\mathbf{k},30\Delta t) \simeq -3$ to ensure a stable base-line level in the last several of the main channels and in the delayed 16 channels. The data were analyzed by curve-fitting $\ln g_1(\mathbf{k},t)$ to a second-order cumulant, i.e., $-\Gamma t + (1/2)\mu_2 t^2$, where $\Gamma$ and $\mu_2$ are the mean and the variance of the decay rate. Selection of the base-line level, either the average of the delayed 16 channels or that using channels 241 to 256, did not alter $\Gamma$ or $\mu_2$ significantly. Using the values of $\Gamma(\mathbf{k})$ for the three scattering angles, we obtained the diffusion coefficients $D_{app}$ for bulk solutions at selected polymer concentrations.

For the polymer chains inside the pores, ACFs were measured at angles 15.8° and 25.5° for samples PS949 and PS170 and at angles 15.8°, 25.5°, and 35.3° for sample PS035. The purpose of our measurements was to obtain the diffusion coefficients in the small $\mathbf{k}$ limit. The values of $|\mathbf{k}|R_P$ at these three angles are 0.11, 0.18, and 0.24, respectively, and therefore the ACFs obtained characterize the dynamics over a distance at least several times the pore radius. The ACFs measured at scattering angles larger than these angles may yield diffusion coefficients different from those determined from the measurements at the smaller scattering angles.[13] Usually two measurements with sampling times $\Delta t$ and $3\Delta t$ were carried out consecutively for the same speckle in the almost nonfluctuating speckle pattern generated by the focused laser beam through the porous glass.[49] The shorter sampling time was selected so that $\ln g_1(\mathbf{k},50\Delta t) \simeq -1$ to ensure a base-line level of long duration in the second measurement with the longer sampling time. For each measurement, the data were accumulated typically for 2000 s. We combined the two ACFs to produce a single ACF. The base-line level was often different from the average level of the delayed 16 channels. However, we could identify the base-line level at channels far delayed from the decay time of the ACF, typically at the last 80 channels of the second measurement. This procedure was repeated several times for different speckles in the speckle pattern.

The combined ACF was analyzed by again curve-fitting $\ln g_1(\mathbf{k},t)$ to a second-order cumulant. The ACFs $g_1(\mathbf{k},t)$ were also analyzed by the program package CONTIN originally provided by Provencher[50] and modified to run on a PC. This program has been widely used for analyzing decay data in general. It deconvolutes an ACF $g_1(\mathbf{k},t)$ to yield the spectrum $G(\Gamma)$ by inverse Laplace transformation:

$$g_1(t) = \int_{\Gamma_{min}}^{\Gamma_{max}} G(\Gamma)\, e^{-\Gamma t}\, d\Gamma \tag{11}$$

where $\Gamma_{min}$ and $\Gamma_{max}$ are the cutoffs for the inverse Laplace transformation. We employed $\Gamma_{max} \simeq 1/\Delta t$ and $\Gamma_{min} \simeq \Gamma_{max}/200$, where $\Delta t$ is the shorter of the sampling times of the two consecutive measurements that were later combined for the analysis. The CONTIN program provides the spectrum $G(\Gamma)$ as a superposition of nonnegative components at selected values of $\Gamma$.

In almost all the data analyzed by the CONTIN program, one of the groups of continuous spectra accounted for more than 98% of the total weight (zeroth moment). The spectrum profile of the main group was sharp, and its average decay rate was identical to that obtained in the cumulant analysis within a few percent at most. In Figure 3, we show a typical example of the CONTIN analysis. A secondary peak was sometimes seen at the high-$\Gamma$ end, because the estimation of $G(\Gamma)$ in this range involves only a few data points and a small amount of noise could be analyzed as a decay component of a large value of $\Gamma$ superimposed on the main decay component. An additional peak at the lower end of $\Gamma$ is related to an error in the estimation of the base line. These secondary peaks were not always observed, even for the same sample and scattering angle that produced them earlier. When they were observed, their heights and positions were different from run to run. They are due to nonsystematic noise

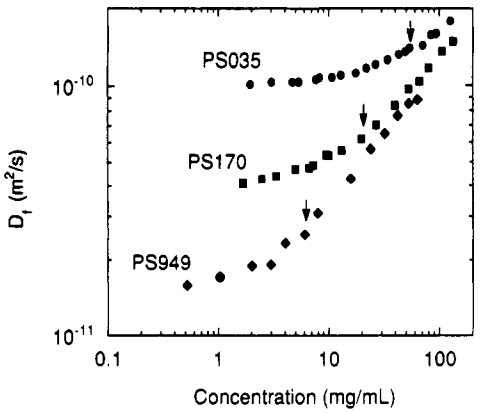


**Figure 1.** Apparent diffusion coefficient $D_f$ corrected for solvent backflow, in free solutions of polystyrene in 2-fluorotoluene plotted against weight concentration expressed in mg/mL for the three samples PS035, PS170, and PS949. Arrows in the figure indicate the overlap concentrations for the three samples.

ascribable to low-frequency vibration or other undesirable noise components and can be neglected.

## Results and Discussion

**Diffusion Coefficients in Free Solutions.** The diffusion coefficients of linear flexible polymers in good solvent have been measured frequently.[32,33,51,52] The purpose of our experiment was purely to obtain a reference for the diffusion inside the pore, to be discussed later in this contribution.

Autocorrelation functions of the light scattered from free solutions of polystyrene in 2FT showed nearly a single-exponential decay for all the samples measured over a wide range of concentrations and for the three scattering angles 15.8°, 25.5°, and 35.3°. The polydispersity index $\mu_2/\Gamma^2$ was less than 1.5% for all the data measured for samples with concentration $\nu \lesssim 3\nu^*$. As the concentration increased, the ACF started to deviate from a single-exponential decay. The ACF for PS949 was also measured at a concentration as high as 123 mg/mL, but a large deviation of $\ln g_1(t)$ from a straight line made it difficult to obtain any specific decay rate in the curve-fitting. Therefore, the data point at the highest concentration for PS949 is excluded from the plot in Figure 1.

Backflow-corrected diffusion coefficients $D_f$ were obtained by fitting the initial decay rate $\Gamma(\mathbf{k})$ to $(1-\phi)D_f\mathbf{k}^2$ for the values measured at the three scattering angles. In Figure 1 we plot $D_f$ against the weight concentration $c$, expressed in mg/mL, for the polystyrene samples PS035, PS170, and PS949. For all three samples, $D_f$ increases as $c$ increases in the whole concentration range studied. We curve-fitted the data to a third-order polynomial to obtain the self-diffusion coefficient $D_0$ extrapolated to zero concentration and the linear coefficient $k_D$ defined in eq 3 with $D_m = D_f$ for the three samples. The values of $k_D$ are all positive, 0.420, 0.630, and 0.771 for PS035, PS170, and PS949, respectively.

The values of $D_0$ obtained in this way are listed in Table I together with the hydrodynamic radius $R_H$ of the respective isolated chain calculated from eq 2. We find that PS949 has a coil radius $R_H \simeq R_P$, whereas PS170 and PS035 have a smaller $R_H$. Note, however, that the radius of gyration $R_g$ is about 50% larger than $R_H$. In terms of $R_g$, the dimensions of PS035 and PS170 in free solutions are smaller than the pore size, whereas the dimension of PS949 is larger, but not excessively so as the scaling theory applies.

We estimate the partition coefficient $p_0$ for the three samples. We assume that $p_0$ is given by eqs 7 and 8

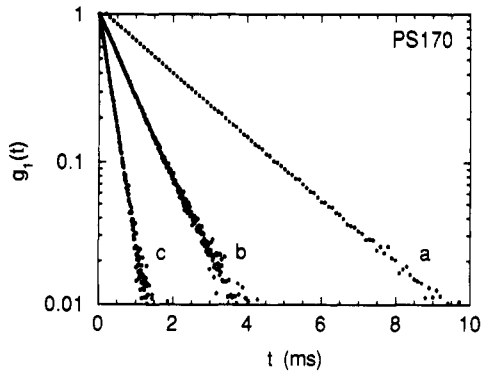


**Figure 2.** Typical heterodyne autocorrelation functions $g_1(t)$ (base-line-subtracted, normalized). Plots a–c are the results from measurements at a scattering angle at 25.5° for sample PS170 at concentrations 3.32, 19.7, and 132 mg/mL which correspond to $c_{out}/c^* = 0.158$, 0.934, and 6.26, respectively.

originally calculated for a Gaussian chain in a straight cylindrical pore;[42] for $R_g$, we use the measured value. Then $p_0$ is estimated to be 0.53, 0.083, and ca. $10^{-7}$ for PS035, PS170, and PS949, respectively. The actual pore has a branched structure and the pore size fluctuates, conditions that make $p_0$ larger, especially for a chain with larger coil radius in free solution.

The arrows in Figure 1 indicate the overlap weight concentrations $c^*$ corresponding to $\nu^*$ that are calculated from $R_g$ (eq 1) for the three samples. The apparent diffusion coefficients $D_f$ of PS170 and PS949 in free solutions show a power dependence on the concentration in the range above $c^*$. For these two samples $D_f$ becomes almost identical for the concentrations above ca. 30 mg/mL, a result indicating that the semidilute regime is realized there and that the decay in the ACF can be ascribed to a cooperative fluctuation in the monomer concentration. The exponent $x$ in eq 5 is estimated to be ca. 0.58, in agreement with the literature values.[32,33,51,52] Any decay constant in the ACF due to translational diffusion of the centers of mass of entangled chains by reptation is expected to be a few orders of magnitude slower[32,33,52] than the decay constant observed here. At high concentration, the increase in $D_f$ slows down. This effect is due to the reptation of entangled chains.[33,35] A small angular dependence of $\Gamma/\mathbf{k}^2$ was also observed at the high concentrations. The data points for PS035 lie above the others. This result is ascribed to the low molecular weight of PS035, which is close to the entanglement molecular weight.

**Diffusion Coefficients in Porous Glasses.** We are concerned here only with the long-wavelength characteristics of the dynamics of polystyrene molecules inside the porous glasses. For PS035 and PS170, the base-line-subtracted heterodyne ACFs $g_1(t)$ measured at the three scattering angles 15.8°, 25.5°, and 35.3° (for PS170, the lower two angles) showed a nearly single-exponential decay for all the concentrations examined. Figure 2 shows examples of the ACFs $g_1(t)$. Plots a–c are ACFs measured at the scattering angle 25.5° for PS170 for three concentrations $c_{out}/c^* = 0.158$, 0.934, and 6.26, where $c_{out}$ is the weight concentration of the polymer outside the pore. The decay rate $\Gamma$ was obtained as an average in the spectrum $G(\Gamma)$ provided by CONTIN. In Figure 3, plots a–c are from spectral analysis of the ACF plots a–c, respectively, in Figure 2. In Figure 3, $\Gamma G(\Gamma)$ represents the spectrum on the logarithmically spaced $\Gamma$. There is a spectral broadening as the concentration increases, although there is still a nearly single-exponential decay observed. The average decay rate obtained in the curve-fitting $g_1(t)$ by

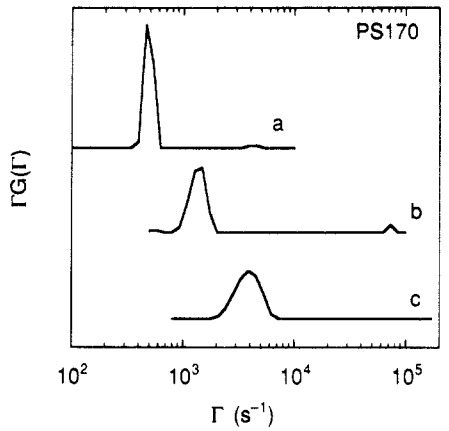


**Figure 3.** Typical spectra obtained in the CONTIN analysis for sample PS170. Plots a–c were obtained for the autocorrelation functions shown by plots a–c, respectively, in Figure 2. On the logarithmic scale, $\Gamma G(\Gamma)$ represents the spectrum.

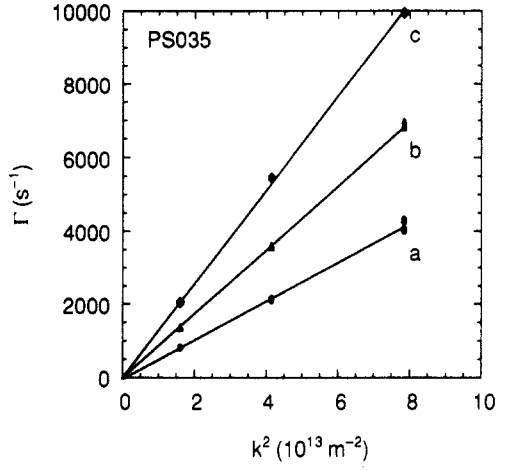


**Figure 4.** Average decay rate $\Gamma$ of the autocorrelation function obtained in the CONTIN analysis for sample PS035 plotted against $\mathbf{k}^2$, where $\mathbf{k}$ is the scattering vector, for three concentrations (a) 10.8, (b) 53.6, and (c) 125 mg/mL.

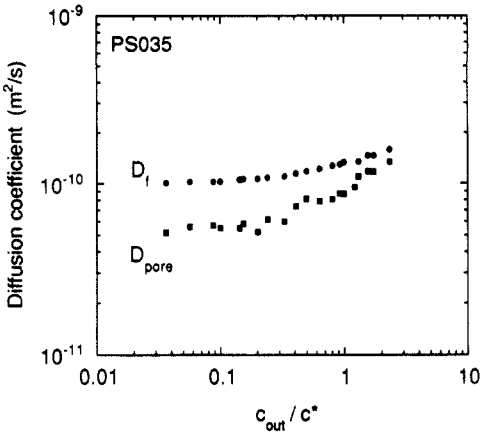


**Figure 5.** Apparent diffusion coefficients $D_{pore}$ inside the controlled pore glasses plotted against the reduced concentration $c_{out}/c^*$ outside the pore for sample PS035. For comparison, values for the solvent backflow-corrected apparent diffusion coefficient $D_f$ in free solution are plotted in the same figure.

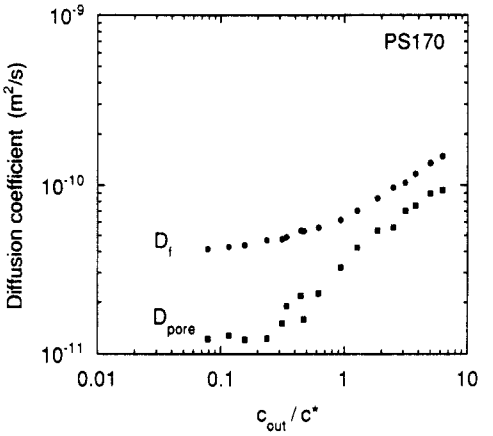


**Figure 6.** Apparent diffusion coefficients $D_{pore}$ inside the controlled pore glasses plotted against the reduced concentration $c_{out}/c^*$ outside the pore for sample PS170. For comparison, values of the solvent backflow-corrected apparent diffusion coefficient $D_f$ in free solution are plotted in the same figure.

the second-order cumulant was in agreement with the average decay rate $\Gamma$ estimated in this way in the CONTIN analysis within an error of at most a few percent.

The apparent diffusion coefficient $D_{pore}$ in the pore was obtained in a plot of $\Gamma$ versus $\mathbf{k}^2$, as shown in Figure 4. This example is for PS035 at three different concentrations: (a) 10.8, (b) 53.6, and (c) 125 mg/mL. The data points obtained from measurements for different speckles are close to each other. The data points for different angles fall around a straight line passing through the origin for each concentration, demonstrating the diffusional behavior of the concentration fluctuation inside the pore. This result was obtained for all the concentration ranges examined for PS035 and PS170. Note that $D_{pore}$ is not corrected for backflow of the solvent, because we do not know the concentration of polymers inside the pore.

For PS949, the ACFs were not consistent with a single-exponential decay at a low concentration range ($c_{out} \lesssim c^*$) and a high concentration range ($c_{out} \gtrsim 3c^*$), athough in the intermediate range, the ACF was close to following a single-exponential decay. The decay rate $\Gamma(\mathbf{k})$ was obtained by fitting a later stage of $\ln g_1(t)$ by a straight line.

It was found that $g_1(t)$ for PS949 is better fitted by a sum of the $\exp(-\Gamma t)$ and the $\exp(2-\Gamma t)$ terms with varying weights, which means that the homodyne component in the heterodyne detection is not negligible for this sample, in particular when the concentration is low. In the intermediate concentration range, the weights for the $\exp(-2\Gamma t)$ terms become as small as 0.1. At a higher concentration, $c_{out} \gtrsim 3c^*$, the ACFs could not be fitted by a sum of the $\exp(-\Gamma t)$ and the $\exp(-2\Gamma t)$ terms, a result suggesting a complicated diffusion mode associated with the entanglement of high molecular weight polymer chains.[32,52] In the high concentration range, the initial decay rate was not proportional to $\mathbf{k}^2$. The apparent diffusion coefficient to be obtained from $\Gamma/\mathbf{k}^2$ was larger at the scattering angle 25.5° than at 15.8°. The discrepancy reached more than 10%, which is to be compared with the difference of a few percent observed in free concentrated solutions of PS949.

Figures 5–7 show a comparison of the apparent diffusion coefficient $D_{pore}$ inside the pore and the diffusion coefficient $D_f$ in free solution for samples PS035, PS170, and PS949, respectively, plotted against $c_{out}/c^*$. Note that $D_f$ is a backflow-corrected value. For all the samples, $D_{pore}$ is almost constant when the concentration is low enough, i.e., when $c_{out}/c^* \lesssim 0.2$, a result indicating a well-defined diluted regime inside the pore. As the concentration increases, $D_{pore}$ increases dramatically above the value for the dilute solution. The increase is more prominent for the larger molecular weight sample. When $c_{out} > c^*$, $D_{pore}$ approaches $D_f$.

The apparent diffusion coefficient $D_{pore}$ for the three samples as a function of monomer concentration outside the pore is shown in Figure 8. The large differences in $D_{pore}$ for different molecular weights, observed in dilute solution, become smaller and almost disappear as the

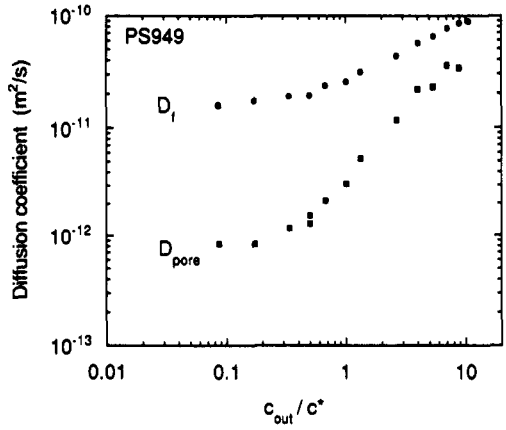


**Figure 7.** Apparent diffusion coefficients $D_{pore}$ inside the controlled pore glasses plotted against the reduced concentration $c_{out}/c^*$ outside the pore for sample PS949. For comparison, values of the solvent backflow-corrected apparent diffusion coefficient $D_f$ in free solution are plotted in the same figure.

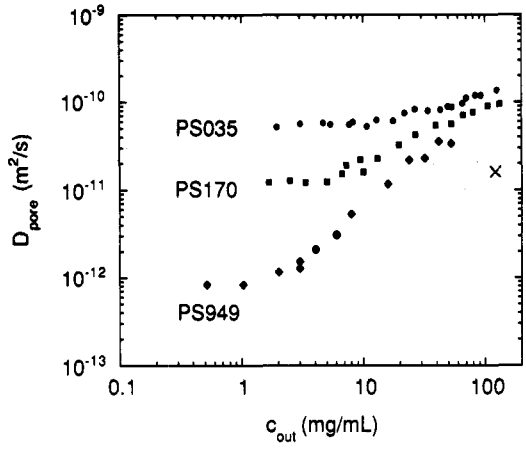


**Figure 8.** Apparent diffusion coefficients $D_{pore}$ of polystyrene solutions inside the controlled pore glasses plotted against the weight concentration $c_{out}$ outside the pore, for the three samples PS035, PS170, and PS949. The symbol "×" in the figure shows the calculated apparent diffusion coefficient of a semidilute polymer solution with a correlation length equal to the pore radius $R_P$ = 275 Å.

concentration reaches ca. 50 mg/mL. Diffusion rates independent of the molecular weight are typical for a semidilute solution. The correlation length $\xi$ estimated by eq 4 with $D_{app} = D_{pore}$ can reach a value much smaller than the pore radius $R_P \simeq 275$ Å. For reference, the symbol "×" was included in Figure 8 to indicate an apparent diffusion coefficient $D_R$ of a semidilute solution with $\xi = R_P$. It is interesting to note that for PS949 the ACFs are close to a single-exponential decay when $D_{pore} \simeq D_R/2$, which gives $\xi \simeq 2R_P = d_P$; the reason is not clear.

Because $D_{pore} > D_R$ and $D_{pore}$ depends only weakly on the molecular weight in the high concentration range, it is more reasonable to consider that the semidilute solution regime is realized within the pore than to ascribe the rapid increase in $D_{pore}$ to any other mechanism, for instance, to enhanced particle–particle interaction in a narrow channel while the concentration inside is still below the overlap concentration. The experimental results here strongly imply a transition from a dilute to a semidilute regime inside the pore as the concentration outside in equilibrium with the pore exceeds $c^*$. The transition is more prominent for a higher molecular weight sample. Below, we will present a theory to explain this transition.

**Scattering Intensity in Porous Glasses.** The heterodyne scattering intensity can also be analyzed in the context of a transition associated with polymer concentration inside the pore. We can utilize the proportionality between the heterodyne coherence factor $f_{HE}$ and the intensity $\langle I_S \rangle$ of light scattered by the polymer molecules inside the porous glasses, as shown in eq 10, if $I_{LO}$ is constant. It was not the case, however. There is a distribution in the refractive indices of the glass beads (some beads appear more translucent in the solutions than do others because of poorer index-matching). Moreover, there is a spatial fluctuation of refractive index within each glass bead, which generates a (nonfluctuating) speckle pattern in the scattering intensity.[49] A particular speckle was chosen as a scattering volume for a run in the heterodyne measurement. In fact, $f_{HE}$ was different from speckle to speckle, even for the same glass bead. Another factor in eq 3 that is not always constant is the coherence factor $f_C$.

There are several factors that produce a deviation in $f_{HE}$, even in different runs with the same sample. This deviation can be overcome by running repetitive measurements and averaging. Panels a–c of Figure 9 are the plots of $f_{HE}$ against the polymer concentration $c_{out}$ outside the pore for the samples PS035, PS170, and PS949, respectively. The measurements were carried out at the scattering angle 25.5°. The arrows in the figures indicate the overlap concentrations $c^*$ for the three samples. As expected, the data are widely scattered. However, there is a correlation between $f_{HE}$ and $c_{out}$. As $c_{out}$ increases, $f_{HE}$ increases while $c_{out} < c^*$, then levels off, and finally decreases for $c_{out} > c^*$. In the ideal condition, which would guarantee $f_{HE} \propto \langle I_S \rangle$, $f_{HE}$ is expected to be proportional to $c_{out}$ for $c_{out} < c^*$, because of a constant partition coefficient. The experimental results, although exhibiting a large fluctuation, appear to be consistent with this prediction. If a semidilute solution regime is realized inside the pore when $c_{out} > c^*$, then $f_{HE}$ is expected to decrease as $f_{HE} \propto \xi^2 \rho_{in} \sim \rho_{in}^{-1/2}$, where $\rho_{in}$ is the monomer concentration inside the pore. Note that $f_{HE}$ is determined by $\rho_{in}$ alone. These experimental results seem to confirm that the semidilute regime is attained in the pore when $c_{out} > c^*$.

**Concentration-Dependent Partition Coefficient.** The experimental results for the apparent diffusion coefficient in the interior of the pore show that the interior solution can attain a semidilute regime, although the partition coefficient $p_0$ for the dilute limit is small. Thus it is reasonable to conclude that there is a transition from the dilute to the semidilute regime as the concentration in the exterior of the pore increases. A scaling theory[27,28,44,45] has been presented for a polymer chain much larger than the pore size, $R_F \gg R_P$, for this nonlinear partitioning. The theory predicts that a transition occurs at a threshold concentration determined by $\xi \sim R_P$, where $\xi$ is the correlation length of the monomer concentration of the exterior polymer solution. The polymer systems in the pore studied here do not satisfy the condition $R_F \gg R_P$. The size of the polymer chain is at best comparable to the pore size. When the exterior concentration reaches the overlap concentration, the correlation length is already smaller than the pore size. Therefore, the threshold concentration in the scaling theory and the transition from weak to strong penetration do not appear to apply to our system. An explanation of the increase in the apparent diffusion coefficient in our system should be based on another argument.

Apparently the transition occurs as the exterior concentration $\nu_{out}$ exceeds ca. $\nu^*$. It is well established in theory[53] and by experiments[29] that monomer–monomer

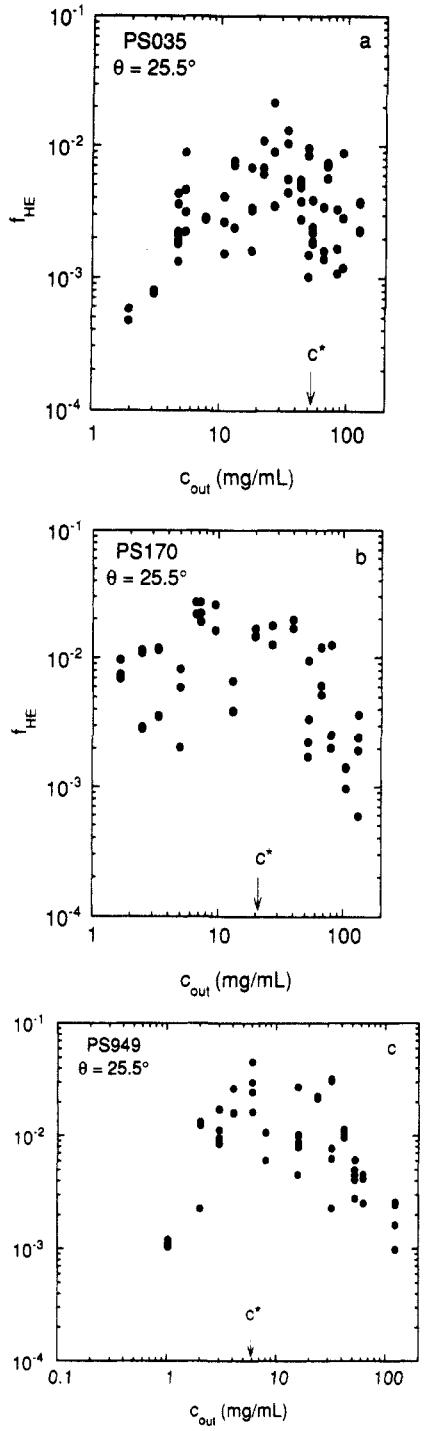


**Figure 9.** Heterodyne coherence factor $f_{HE}$ plotted against weight concentration $c_{out}$ outside the pore for (a) PS035, (b) PS170, and (c) PS949. All the data points shown here measured at a scattering angle of 25.5°. The arrows indicate the overlap concentrations $c^*$ for the three samples.

interaction causes the osmotic pressure to increase rapidly in free solutions as the solute concentration exceeds ca. $\nu^*$. At this point it becomes easier for a chain to escape into the pore in which the osmotic pressure is lower even though the configurational entropy is smaller than that outside the pore. Thus the partition coefficient $p_I$ begins to be larger than its value at infinite dilution $p_0$. To estimate quantitatively how $p_I$ changes as a function of $\nu_{out}$, we need to develop expressions for the chemical potentials of a chain in the interior and the exterior of the pore.

Using renormalization group theory, intensive research has been carried out[34,53-56] to obtain an expression for the osmotic pressure $\Pi_{out}$ of linear-chain molecules in free solution with short-range repulsive interaction between monomers over a wide range of concentrations. Here we use a useful approximate expression obtained by Ohta and Oono[56] for the osmotic pressure that covers a wide range of $\nu_{out}$:

$$\Pi_{out}/\nu_{out}k_BT = P(X_{out}) \tag{12}$$

where $P(X)$ is given as

$$P(X) \equiv 1 + \frac{1}{2}X \exp\left\{\frac{1}{4}\left[\frac{1}{X} + \left(1 - \frac{1}{X^2}\right)\ln(1+X)\right]\right\} \tag{13}$$

and the reduced concentration $X_{out}$ is proportional to $\nu_{out}/\nu^*$. When $X_{out} \gg 1$, eq 12 yields $\Pi_{out} \propto X_{out}^{9/4}$, a relation obtained in the scaling argument.[29] To evaluate the numerical factor connecting $X_{out}$ and $\nu_{out}/\nu^*$, we compare the second virial coefficient in eqs 12 and 13 with its counterpart in a virial expansion for $\Pi_{out}$ derived for a sufficiently long chain with a short-range repulsive force:[57-60]

$$\frac{\Pi_{out}}{\nu_{out}k_BT} = 1 + \frac{1}{2}g^*(2\pi)^{3/2}\nu_{out}\left(\frac{1}{3}R_F^2\right)^{3/2} + \dots \tag{14}$$

where $g^*$ represents the effective interaction between monomers in the long-chain limit. Comparing terms linear in $\nu_{out}$ in eqs 12 and 14, we obtain

$$X = e^{-1/8}g^*\left(\frac{\pi}{3}\right)^{3/2\nu_{out}}\left(\frac{R_F}{R_g}\right)^3 = e^{-1/8}g^*\left(\frac{2\pi}{\mathcal{N}}\right)^{3/2\nu_{out}} \tag{15}$$

where the ratio $\mathcal{N} \equiv 6R_g^2/R_F^2$ is defined for an isolated long chain with hard-core repulsion. Using $g^* = 0.233$[61] and $\mathcal{N} = 0.952$,[40,41] we arrive at

$$X_{out} \simeq 3.49\nu_{out}/\nu^* \tag{16}$$

The chemical potential $\mu_{out}$ is then calculated as the free energy per chain

$$\mu_{out}/k_BT = P(X_{out}) - \int d(X_{out}^{-1})X_{out}P(X_{out}) = \ln \nu_{out} + I(X_{out}) \tag{17}$$

where a reference concentration for the first term, the chemical potential of an ideal solution, is $\nu_{out} = 1$. The interaction term $I(X_{out})$ is defined by

$$I(X_{out}) \equiv P(X_{out}) - 1 + \int_0^{X_{out}} \frac{P(x) - 1}{x}\,dx \tag{18}$$

where $X_{out} = 0$ was chosen for the reference.

The short-range monomer–monomer interaction causes a deviation of the osmotic pressure $\Pi_{out}$ from that of an ideal solution. This interaction exists also in the pore. A difference between the chain conformation in the pore and that outside the pore, however, can result in a change in the average interaction that the monomer perceives from other monomers either on the same chain or on other chains. We denote the average interactions in the interior and exterior of the pore as $U_{in}$ and $U_{out}$, respectively. In the following, we estimate the difference.

For a short chain with $R_g < R_P$, the functional form for $U_{in}$ is the same as $U_{out}$. Thus we need only consider the interaction for a chain with $R_g > R_P$, which can be done in the two concentration ranges separately. When $\nu_{in} > \nu_{in}^*$ ($\nu_{in}^*$ is the overlap polymer concentration inside the pore), on the one hand, most of the pair interaction is between monomers within the distance of the correlation length, which is smaller than the pore radius. Thus $U_{in}$ has the same functional form as $U_{out}$. When $\nu_{in} < \nu_{in}^*$, on

the other hand, the interaction should show some change. The ratio of $U_{in}$ to $U_{out}$ is equal to the ratio of the monomer concentration $\bar{\rho}_{in}$ inside the volume occupied by a polymer chain inside the pore to $\bar{\rho}_{out}$, that in the bulk solution. Then $U_{in}/U_{out} = \bar{\rho}_{in}/\bar{\rho}_{out} \simeq R_F^3/(R_P^2 R_\parallel) \simeq (R_F/R_P)^{4/3}$, where the results $R_F = aN^{3/5}$ and eq 9 were used.

The power $^4/_3$ is reasonably close to unity. Therefore, except for a very long polymer molecule in dilute solution, the same expression can be used for the interaction term in the chemical potential for a chain inside the pore. We also note that $\nu_{in}^* \simeq \nu_{out}^*$ for a chain extended over a length at most comparable to the pore size. Therefore in the following we use the same overlap concentration for both the interior of the pore and the exterior. Thus we can write the chemical potential $\mu_{in}$ of a polymer chain in the pore as

$$\mu_{in}/k_BT = \ln \nu_{in} + I(X_{in}) + \Delta S/k_B \qquad (19)$$

where the reference term for the ideal solution is set at $\nu_{in} = 1$. Here it is assumed that the pore is homogeneous and therefore $\mu_{in}$, $\nu_{in}$, and $\Delta S$ are constant throughout the pore space (below we will consider inhomogeneity).

Note that $\Delta S$ also depends on the concentration. Polymer chains in good solvents contract as the concentration increases because of the screening of monomer–monomer interaction.[62,63] Ohta and Oono[56] also proposed an approximate expression for the normalized root-mean-square end-to-end distance $R_F$ as a function of concentration:

$$\frac{R_F(X)}{R_{F0}} = \exp\left\{\frac{1}{16}X\left[\frac{3}{Y} - \left(\frac{3}{2Y^2} + \frac{1}{Y}\right)(\gamma + \ln 2Y) + e^{2Y}\,\mathrm{Ei}\,(-2Y)\left(1 - \frac{2}{Y} + \frac{3}{2Y^2}\right)\right]\right\} \qquad (20)$$

where $R_{F0}$ is the value of $R_F$ in the dilute limit, $Y = 1 + X$, $\gamma \simeq 0.5772$ is Euler's constant, and $\mathrm{Ei}\,(-x) \equiv -\int_x^\infty [\exp(-t)/t]\,dt$.

For simplicity, we assume that the expression for the entropy reduction due to confinement for a Gaussian chain[42] applies also for a real chain in a good solvent, if we use the radius of gyration of the real chain for $R_g$ in eqs 7 and 8. It is well-known that the ratio of $R_g$ to $R_F$ is insensitive to the excluded volume.[56] Therefore $R_g/R_{g0} = R_F/R_{F0}$, where $R_{g0}$ is the value of $R_g$ in the dilute limit. Thus we can express the entropy reduction as

$$\frac{\Delta S}{k_B} = -\ln f_P\left(\frac{R_{g0}}{R_P}\frac{R_F(X_{in})}{R_{F0}}\right) \qquad (21)$$

where $f_P$ is given by eq 8.

We impose the condition of balance, $\mu_{in} = \mu_{out}$, and from eqs 17, 19, and 21, we obtain the partition coefficient $p_I$ as

$$p_I = \frac{\nu_{in}}{\nu_{out}} = \frac{X_{in}}{X_{out}} = f_P\left(\frac{R_{g0}}{R_P}\frac{R_F(X_{in})}{R_{F0}}\right)\exp[I(X_{out}) - I(X_{in})] \qquad (22)$$

By solving eq 22 self-consistently, we can obtain $p_I$ or $X_{in}$ as a function of $X_{out}$ and $p_0 = f_P(R_{g0}/R_P)$. In the dilute limit, $p_I \simeq p_0[1 + e^{1/8}(1 - p_0)X_{out}]$, which reproduces a peaking[26] in the linear coefficient of $p_I$ with respect to $p_0$.

In Figure 10, we plotted $p_I$ against $X_{out}$ in double-logarithmic scale for several values of $p_0$. They are, from top to bottom, $3.16 \times 10^{-1}$, $1 \times 10^{-1}$, $3.16 \times 10^{-2}$, $1 \times 10^{-2}$, $3.16 \times 10^{-3}$, $1 \times 10^{-3}$, $3.16 \times 10^{-4}$, $1 \times 10^{-4}$, $3.16 \times 10^{-5}$, and $1 \times 10^{-5}$. These values correspond to $R_{g0}/R_P = 0.381, 0.585, 0.736, 0.861, 0.970, 1.068, 1.157, 1.240, 1.318$, and $1.391$, respectively. For all values of $p_0$, $p_I$ increases rapidly as $\nu_{out}$ exceeds $\nu^*$ ($X_{out} \simeq 3.49$) and finally approaches unity as $\nu_{out} \to \infty$. Details of the increase of $p_I$ are seen in Figure 11, which plots $p_I$ against $X_{out}$ on a linear scale (only curves for $p_0 = 10^{-1}, 10^{-2}, 10^{-3}, 10^{-4}$, and $10^{-5}$ are shown). These plots thus explain the transition of the interior solute concentration at least qualitatively.

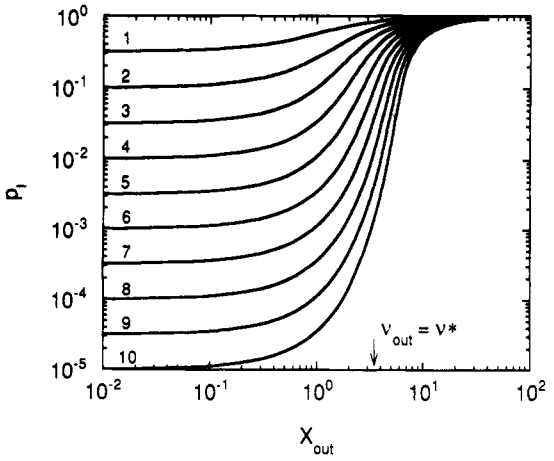


**Figure 10.** Partition coefficient $p_I$ plotted against the reduced polymer concentration $X_{out} = (\nu_{out}/\nu^*) \times 3.49$ outside the pore, for selected values of $p_0$, the value of $p_I$ in the dilute limit $X_{out} \ll 1$. The values of $p_0$ are, from top to bottom, (1) $3.16 \times 10^{-1}$, (2) $1 \times 10^{-1}$, (3) $3.16 \times 10^{-2}$, (4) $1 \times 10^{-2}$, (5) $3.16 \times 10^{-3}$, (6) $1 \times 10^{-3}$, (7) $3.16 \times 10^{-4}$, (8) $1 \times 10^{-4}$, (9) $3.16 \times 10^{-5}$, and (10) $1 \times 10^{-5}$.

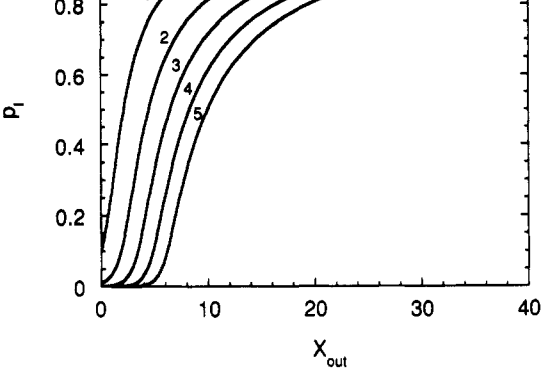


**Figure 11.** Partition coefficient $p_I$ plotted against the reduced polymer concentration $X_{out} = (\nu_{out}/\nu^*) \times 3.49$ outside the pore on a linear scale. The values of $p_0$, the value of $p_I$ in the dilute limit $X_{out} \ll 1$, are, from top to bottom, (1) $10^{-1}$, (2) $10^{-2}$, (3) $10^{-3}$, (4) $10^{-4}$, and (5) $10^{-5}$.

To compare two factors contributing to the increase in $p_I$, we also calculated the entropy factor $\ln (f_P/p_0)$ and the osmotic pressure factor $I(X_{out}) - I(X_{in})$ separately (see eq 22; both factors on a logarithmic scale). For all values in the plot in Figure 10, the entropic factor surpasses the other factor. Their difference is smaller for a smaller $p_0$ and a larger $X_{out}$. At its smallest, the difference was about 1.03 ($X_{out} = 40$, $p_0 = 1 \times 10^{-5}$), and the size of the chain at that condition is $R_g/R_P \simeq 1.19$ (cf. $R_{g0}/R_P \simeq 1.391$). The entropic factor due to the chain contraction plays a minor role. Thus the increase in the concentration inside the pore was found to be ascribed primarily to the increased osmotic pressure outside the pore. For a polymer chain, it is easier to escape into the pore, even at the expense of reduced configurational entropy, than to withstand the high osmotic pressure outside the pore.

By the same mechanism that causes increased inflow of polymer molecules into the pore at higher concentrations, a distribution of pore size in the network can change the

cooperative diffusion coefficient $D_C$ of a polymer molecule in the pore as detected by heterodyne DLS. We note that in heterodyne detection a component in the signal intensity decaying by the factor $\exp(-D_C\mathbf{k}^2t)$ is proportional to the scattering intensity $I_S$ from the polymer, which in turn is proportional to $\xi^2\rho$, where the correlation length $\xi$ and the monomer concentration $\rho$ are functions of position along the interwinding network pore channels. They are coarse grained on the scale of the pore radius. Because $D_C$ is proportional to $1/\xi$, the expected value $\langle D_C\rangle$ in the heterodyne DLS is related to $\bar{D}_C$, the ideal value of $D_C$ for monodisperse pore size, by

$$\frac{\langle D_C\rangle}{\bar{D}_C} = \frac{\bar{\xi}\langle\xi\rho\rangle}{\langle\xi^2\rho\rangle} \cong 1 - \frac{15}{32}\frac{\langle\Delta\rho^2\rangle}{\bar{\rho}^2} \tag{23}$$

where $\Delta\rho = \rho - \bar{\rho}$, $\bar{\xi}$ and $\bar{\rho}$ are the values of $\xi$ and $\rho$ for monodisperse pore size, and $\xi \sim \rho^{-3/4}$ for the semidilute regime was used. Thus a distribution in the monomer concentration due to a small distribution of pore sizes always reduces the cooperative diffusion coefficient $\langle D_C\rangle$ as detected by DLS.

To relate $\Delta R_P$, the deviation of $R_P$ from the average value $\bar{R}_P$, to $\Delta\rho$, we have to consider an equilibrium equation along the pore space:

$$I\left(\frac{7}{2}\rho/\rho^*\right) + \ln\rho - \ln f_P(R_g/R_P) = I\left(\frac{7}{2}\bar{\rho}/\rho^*\right) + \ln\bar{\rho} - \ln f_P(R_g/\bar{R}_P) \tag{24}$$

where $^7/_2$ was used for the conversion of $\rho/\bar{\rho}$ to $X$ (see eq 16), and a fluctuation of the coil radius $R_g$ along the pore space is neglected. In the semidilute regime, $I(X) \cong \frac{9}{10}X^{5/4}$. If we approximate $-\ln f_P(x) \cong \beta_1^2x^2$, we get

$$\frac{\Delta\rho}{\bar{\rho}} = \frac{-2\ln f_P(R_g/\bar{R}_P)}{1 + \frac{9}{8}\left(\frac{7}{2}\bar{\rho}/\rho^*\right)^{5/4}}\frac{\Delta R_P}{\bar{R}_P} \tag{25}$$

The absolute value of the relative deviation $\Delta\rho/\bar{\rho}$ is larger for a smaller $f_P(R_g/\bar{R}_P)$, i.e., a higher molecular weight sample, and a smaller concentration $\bar{\rho}/\rho^*$. Combining eqs 23 and 25, we find a decrease in $\langle D_C\rangle$ due to nonuniform pore size is more prominent for a higher molecular weight sample and at a smaller concentration.

If both the solutions in the interior and the exterior of the pore are semidilute, the ratio of the two cooperative diffusion coefficients should lead to the ratio of the correlation length, which is a function of monomer concentration. Assuming $\xi \sim \rho^{-3/4}$, we obtain $p_1 = \rho_{in}/\rho_{out} = (D_{pore}/D_f)^{4/3}$.

In Figure 12, we plot $(D_{pore}/D_f)^{4/3}$ against $c_{out}/c^*$, which can be compared with Figure 11. Note that the $D_f$ is backflow corrected, whereas $D_{pore}$ is not. As $c_{out}/c^*$ exceeds 1, $(D_{pore}/D_f)^{4/3}$ shows a rapid increase. In the range $1 < c_{out}/c^* < 2$, the plots for the three polystyrene samples seem to follow the transition curve in Figure 11. At a higher concentration, the plots show a saturation toward values below unity, a result that is not consistent with Figure 11. This discrepancy is ascribable to the distribution in pore size, hydrodynamic interaction between polymer chains and pore walls, and a contribution of the reptation mode; the discrepancy is larger for a polystyrene sample of higher molecular weight.

## Concluding Remarks

Applying the technique of dynamic light scattering to nearly perfectly index-matched samples of polystyrene solutions in controlled pore glasses, we found that the apparent diffusion coefficient of the polymer molecule inside the pore shows a rapid increase as the concentration outside the pore exceeds the overlap concentration. The increase was more prominent for a polymer chain of higher molecular weight that has a smaller partition coefficient in the dilute limit. The correlation length obtained from the diffusion coefficient, assuming a cooperative diffusion mode for polymer solutions inside the pore, reached a value smaller than the pore radius. The correlation length does not depend on the molecular weight but depends on the monomer concentration alone. These features demonstrate the realization of a semidilute regime within the porous glass. The transition in the concentration can be ascribed to a rapid increase in the osmotic pressure outside the pore as the concentration there exceeds the overlap concentration and to the consequent penetration of polymer chains into the pore network. The effect of chain contraction in the semidilute regime was found to be smaller than that of the osmotic pressure.

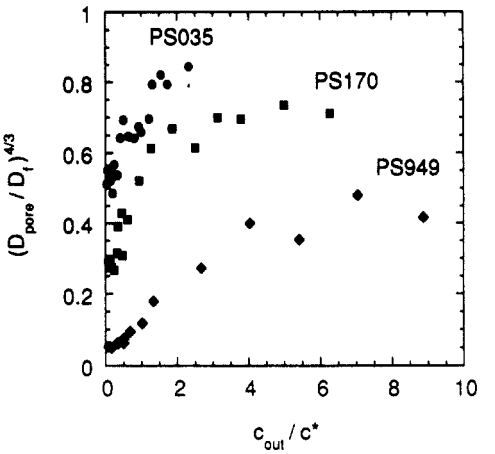


**Figure 12.** Factor $(D_{pore}/D_f)^{4/3}$ plotted against $c_{out}/c^*$ for comparison with Figure 11. Note that $D_f$ is backflow corrected, whereas $D_{pore}$ is not. In the semidilute regime, $(D_{pore}/D_f)^{4/3}$ is expected to be equal to the partition coefficient.

In this study we focused on the cooperative diffusion mode. From the effect of angular dependence of the apparent diffusion coefficient for higher molecular weight samples, it is clear that more studies should be carried out over a wide range of scattering vectors to elucidate the involvement of the reptation mode in the chain dynamics inside the pore. Other interesting extensions could include the transitional behavior of polymer molecules of other architectures, e.g., rigid-chain polymers that show isotropic–nematic phase transitions and spherical polymers that exhibit an interaction different from that of linear-chain polymers.

**Acknowledgment.** This work was supported in part by the Air Force Office of Scientific Research Grant No. 91-001. We also acknowledge Shell Development Co. for supplying the porous glass beads.

## References and Notes

(1) Yau, W. W.; Kirkland, J. J.; Bly, D. D. In *High Performance Liquid Chromatography*; Brown, P. R., Hartwick, R. A., Eds.; John Wiley: New York, 1989; Vol. 98; pp 277–316.
(2) Giddings, J. C. *Unified Separation Science*; John Wiley: New York, 1991.
(3) Colin, H. In *High Performance Liquid Chromatography*; Brown, P. R., Hartwick, R. A., Eds.; John Wiley: New York, 1989; Vol. 98; pp 415–478.
(4) Cannell, D. S.; Rondelez, F. *Macromolecules* **1980**, *13*, 1599.
(5) Guillot, G.; Léger, L.; Rondelez, F. *Macromolecules* **1985**, *18*, 2531.

(6) Bohrer, M. P.; Patterson, G. D.; Carroll, P. J. *Macromolecules* **1984**, *17*, 1170.
(7) Bohrer, M. P.; Feters, L. J.; Grizzuti, N.; Pearson, D. S.; Tirrell, M. V. *Macromolecules* **1987**, *20*, 1827.
(8) Guillot, G. *Macromolecules* **1987**, *20*, 2600.
(9) Guillot, G. *Macromolecules* **1987**, *20*, 2606.
(10) Davidson, M. G.; Deen, W. M. *J. Membr. Sci.* **1988**, *35*, 167.
(11) Davidson, M. G.; Deen, W. M. *Macromolecules* **1988**, *21*, 3474.
(12) Bishop, M. T.; Langley, K. H.; Karasz, F. E. *Phys. Rev. Lett.* **1986**, *57*, 1741.
(13) Bishop, M. T.; Langley, K. H.; Karasz, F. E. *Macromolecules* **1989**, *22*, 1220.
(14) Easwar, N.; Langley, K. H.; Karasz, F. E. *Macromolecules* **1990**, *23*, 738.
(15) Guo, Y.; Langley, K. H.; Karasz, F. E. *Macromolecules* **1990**, *23*, 2022.
(16) Guo, Y.; Langley, K. H.; Karasz, F. E. *Macromolecules* **1992**, *25*, 4902.
(17) Guo, Y.; Langley, K. H.; Karasz, F. E., submitted for publication in *Phys. Rev. B*.
(18) Guo, Y.; O'Donohue, S. J.; Langley, K. H.; Karasz, F. E. *Phys. Rev. A* **1992**, *46*, 3335.
(19) Sahimi, M.; Jue, V. L. *Phys. Rev. Lett.* **1989**, *62*, 629.
(20) Anderson, J. L.; Quinn, J. A. *Biophys. J.* **1974**, *14*, 130.
(21) Bleha, T.; Mlýnek, J.; Berek, D. *Polymer* **1980**, *21*, 798.
(22) Bleha, T.; Spychaj, T.; Vondra, R.; Berek, D. *J. Polym. Sci., Polym. Phys. Ed.* **1983**, *21*, 1903.
(23) Cifra, P.; Bleha, T.; Romanov, A. *Makromol. Chem., Rapid Commun.* **1988**, *9*, 355.
(24) Cifra, P.; Bleha, T.; Romanov, A. *Polymer* **1988**, *29*, 1664.
(25) Bleha, T.; Cifra, P.; Karasz, F. E. *Polymer* **1990**, *31*, 1321.
(26) Brannon, J. H.; Anderson, J. L. *J. Polym. Sci., Polym. Phys. Ed.* **1982**, *20*, 857.
(27) Brochard, F.; de Gennes, P.-G. *J. Chem. Phys.* **1977**, *67*, 52.
(28) Daoudi, S.; Brochard, F. *Macromolecules* **1978**, *11*, 751.
(29) Daoud, M.; Cotton, J. P.; Farnoux, B.; Jannink, G.; Sarma, G.; Benoit, H.; Duplessix, R.; Picot, C.; de Gennes, P.-G. *Macromolecules* **1975**, *8*, 804.
(30) Adam, M.; Delsanti, M. *Macromolecules* **1977**, *10*, 1229.
(31) Schaefer, D. W.; Joanny, J. F.; Pincus, P. *Macromolecules* **1980**, *13*, 1280.
(32) Amis, E. J.; Han, C. C. *Polymer* **1982**, *23*, 1403.
(33) Schaefer, D. W.; Han, C. C. In *Dynamic Light Scattering*; Pecora, R., Ed.; Plenum Press: New York, 1985; pp 181–243.
(34) des Cloizeaux, J.; Jannink, G. *Polymers in Solution: Their Modelling and Structure*; Clarendon Press: Oxford, U.K., 1990.
(35) Doi, M.; Edwards, S. F. *The Theory of Polymer Dynamics*; Clarendon Press: Oxoford, U.K., 1986.
(36) Schmitz, K. S. *An Introduction to Dynamic Light Scattering by Macromolecules*; Academic Press: San Diego, 1990.
(37) Geissler, E.; Hecht, A. M. *J. Phys. (Paris)* **1979**, *40*, L-173.
(38) There is still a controversy about the backflow corrections. Here we employ a correction factor of $1 - \phi$.
(39) Oono, Y.; Kohmoto, M. *J. Chem. Phys.* **1983**, *78*, 520.
(40) Witten, T. A.; Schäfer, L. *J. Phys. A.* **1978**, *11*, 1843.
(41) Benhamou, M.; Mahoux, G. *J. Phys. (Paris)* **1985**, *46*, L-689.
(42) Casassa, E. F. *J. Polym. Sci., Polym. Lett. Ed.* **1967**, *5*, 773.
(43) Giddings, J. C.; Kucera, E.; Russell, C. P.; Myers, M. N. *J. Phys. Chem.* **1968**, *72*, 4397.
(44) Daoud, M.; de Gennes, P.-G. *J. Phys. (Paris)* **1977**, *38*, 85.
(45) de Gennes, P.-G. *Scaling Concepts in Polymer Physics*; Cornell University Press: Ithaca, NY, 1979.
(46) Siegert, A. J. F. *MIT Radiation Lab. Report* **1943**, 465.
(47) Chu, B. *Laser Light Scattering*; Academic Press: San Diego, 1991.
(48) Hert, M.; Strazielle, C.; Benoit, H. *Macromol. Chem.* **1973**, *172*, 169.
(49) Pusey, P. N.; van Megen, W. *Physica A* **1989**, *157*, 705.
(50) Provencher, S. W. *Macromol. Chem.* **1979**, *180*, 201.
(51) Brown, W.; Nicolai, T. *Colloid Polym. Sci.* **1990**, *268*, 977.
(52) Eisele, M.; Burchard, W. *Macromolecules* **1984**, *17*, 1636.
(53) des Cloizeaux, J. *J. Phys. (Paris)* **1975**, *36*, 281.
(54) des Cloizeaux, J. *J. Phys. (Paris)* **1980**, *41*, 749.
(55) Knoll, A.; Schäfer, L.; Witten, T. A. *J. Phys. (Paris)* **1981**, *42*, 767.
(56) Ohta, T.; Oono, Y. *Phys. Lett.* **1982**, *89A*, 460.
(57) Yamakawa, H. *J. Phys. Soc. Jpn.* **1958**, *13*, 87.
(58) Kurata, M.; Yamakawa, H. *J. Chem. Phys.* **1958**, *29*, 311.
(59) Kurata, M.; Fukatsu, M.; Satobayashi, H.; Yamakawa, H. *J. Chem. Phys.* **1964**, *41*, 139.
(60) Casassa, E. F. *J. Chem. Phys.* **1959**, *31*, 800.
(61) des Cloizeaux, J. *J. Phys. (Paris)* **1981**, *42*, 635.
(62) Edwards, S. F. *J. Phys. A.* **1975**, *8*, 1670.
(63) Edwards, S. F.; Jeffers, E. F. *J. Chem. Soc., Faraday Trans. 2* **1979**, *33*, 1020.